Annual Review of Control, Robotics, and Autonomous Systems

Motion Control in Magnetic Microrobotics: From Individual and Multiple Robots to Swarms

Lidong Yang and Li Zhang

Department of Mechanical and Automation Engineering, The Chinese University of Hong Kong, Hong Kong SAR, China; email: ldyang@mae.cuhk.edu.hk, lizhang@mae.cuhk.edu.hk

Annu. Rev. Control Robot. Auton. Syst. 2021. 4:509–34

First published as a Review in Advance on November 6, 2020

The *Annual Review of Control, Robotics, and Autonomous Systems* is online at control.annualreviews.org

https://doi.org/10.1146/annurev-control-032720-104318

Keywords

magnetic microrobots, motion control, multiagent control, swarm control, closed-loop control at microscale

Abstract

Magnetic microrobotics has undergone approximately 20 years of development, and the robotics and control communities have contributed significant theoretical and practical results to the motion control aspects of this field. This article introduces fundamental motion principles covering individual, multiagent, and swarm control and critically reviews the state of the art along with representative results. It then describes closed-loop control (an important part of this field), including the system structure, current motion planning and control methods, and current feedback approaches. As the development of motion control in magnetic microrobotics is far from complete, especially for swarm control, its current limitations are discussed. Finally, we conclude with several challenges and future research directions.

1. INTRODUCTION

Mobile robotics at micro- and nanoscales has become a popular field with significant value. New actuation principles and control theories have been established (1, 2), and broad biomedical applications have been explored (3, 4). A variety of fuel-free actuation principles (5)—including optical, (6), chemical (7), ultrasound (8), electrostatic (9), and magnetic (10) approaches—have now been proposed that enable microrobots to navigate in narrow and enclosed fluidic spaces. Among these approaches, magnetic actuation has intrinsic advantages because magnetic fields are transparent and safe for biological tissues. In addition, an external magnetic manipulation system can wirelessly transfer actuation power to microrobots that have very limited space for onboard energy. The features of magnetic microrobots that are favorable for biomedicine have led to the rapid expansion of the field of magnetic microrobotics. Thanks to the innovation and efforts of researchers, many recent successes have demonstrated the great potential of magnetic microrobots in biomedical applications (11–14).

As an interdisciplinary subject, magnetic microrobotics combines materials science, micro- and nanofabrication, robotics and control, and more. Within these areas, motion control technology enables the development of magnetic microrobots with various controllable motion modalities, high motion accuracy (closed-loop control), and high task efficiency (motion planning). These advances promote real microrobotics applications in environments that may be complex and dynamic. This article focuses on motion control in magnetic microrobotics, including individual, multiagent, and swarm control. It reviews principles of motion, the state of the art, and closed-loop control, with an emphasis on swarm control, an emerging and challenging topic in magnetic microrobotics. In fact, owing to the small volumes and surface areas of individual microrobots, microrobotic cargo delivery tasks could require a swarm of microrobots (15, 16). In vivo tracking of a single microrobot is another issue because of insufficient imaging resolution (17).

To limit the scope of this review, we do not cover other important aspects of magnetic microrobotics that have been covered by several other review articles, such as magnetic actuation and the corresponding magnetic manipulation systems (18–20), magnetic microrobots with soft components (21), magnetic microrobot design with biohybrid actuation (22), and micromanipulation using magnetic microrobots (23). The article has four main objectives: (*a*) to present the motion principles of individual magnetic microrobots and discuss what strategies can be utilized to extend them in order to realize multiagent and swarm control; (*b*) to critically review and compare representative control results for individual, multiagent, and swarm magnetic microrobots; (*c*) to introduce closed-loop motion control of magnetic microrobots so that readers will understand the research to date and how to construct such a system for their own applications; and (*d*) to discuss current limitations and provide future perspectives on this field.

We start in Section 2 by describing the dominating forces and torques exerted on magnetic microrobots; Section 3 then summarizes the classic motion principles of individual magnetic microrobots based on these forces or torques and the strategies that can be adopted to extend them to multiagent or swarm control. Section 4 thoroughly reviews the motion control principles for multiple magnetic microrobots and swarms of magnetic microrobots and provides a time line of representative results. Section 5 outlines the system structure for closed-loop control of magnetic microrobots and references representative works. Finally, a conclusion and future perspectives are presented in Section 6.

2. DOMINATING FORCES AND TORQUES ON MAGNETIC MICROROBOTS

In the film *Fantastic Voyage*, a team of scientists and their submarine are shrunk to microscale and must navigate through human blood vessels to save the life of a dying man. However, according

to the scaling law (24), the structures of both the humans and the submarine would be highly vulnerable after miniaturization, and the locomotion methods of human walking and propeller propulsion would no longer work. The motion of microobjects is dominated by viscous dissipation and the absence of inertia, which can be quantified by the Reynolds number (*Re*) of the flow:

$$Re = \frac{\rho v L}{\mu}, \qquad 1.$$

where ρ, v, and μ represent the density, flow velocity, and dynamic viscosity of the fluid, respectively, and L is the characteristic length of the object. The working environment of magnetic microrobots often has a low Reynolds number ($Re \ll 1$), and the robots' design must account for the applicable motion principles (25).

In a fluid, two types of forces and torques dominate the motion of magnetic microrobots: magnetic and fluidic. If the robots move near a boundary, the wall effect and boundary forces also contribute to their motion. Note that these forces and torques usually cannot be independently controlled. In magnetic microrobotics, magnetic forces and torques are often the only control inputs of a microrobotic system, whose dynamic control activates the variations of the other forces and torques on the microrobot so that the net force and torque lead to the desired motion.

2.1. Magnetic Forces and Torques

This subsection describes the magnetic forces and torques exerted on magnetic microrobots when they are actuated by magnetic fields.

2.1.1. Global magnetic force and torque. When a magnetic microrobot is placed in a magnetic field with a strength vector of $\mathbf{B}$ (unit T), a global magnetic force $\mathbf{F}_{\text{gmag}}$ (unit N) is exerted on it that can be computed as

$$\mathbf{F}_{\text{gmag}} = (\mathbf{m} \cdot \nabla)\mathbf{B} = \left[\frac{\partial \mathbf{B}}{\partial x} \; \frac{\partial \mathbf{B}}{\partial y} \; \frac{\partial \mathbf{B}}{\partial z}\right]^{\mathrm{T}} \mathbf{m}, \qquad 2.$$

where $\mathbf{m}$ (unit A·m^2) is the magnetic moment of the microrobot. In addition, a global magnetic torque $\boldsymbol{\tau}_{\text{gmag}}$ (unit N·m) will be applied on the microrobot:

$$\boldsymbol{\tau}_{\text{gmag}} = \mathbf{m} \times \mathbf{B} = Sk(\mathbf{m})\mathbf{B} = \begin{bmatrix} 0 & -m_z & m_y \\ m_z & 0 & -m_x \\ -m_y & m_x & 0 \end{bmatrix} \mathbf{B}, \qquad 3.$$

where $Sk(\cdot)$ represents the skew-symmetric matrix of a vector. Petruska & Nelson (26) and Mahoney & Abbott (27) described how to generate and control $\mathbf{F}_{\text{gmag}}$ and $\boldsymbol{\tau}_{\text{gmag}}$ by using an electromagnetic system and a permanent magnet system, respectively.

2.1.2. Interactive magnetic force and torque. For a group of magnetic microrobots, the interactive magnetic forces and torques among them are also significant for their individual motions. It is reasonable to approximate the magnetic microrobots as dipoles in many cases—for example, when the microrobot has a nearly spherical shape or when the distance between two microrobots is large enough (e.g., >1.5 body lengths) (28). Under this approximation, the interaction force and torque on the ith microrobot in a group of N magnetic microrobots can be computed using Equations 4 and 5, respectively:

$$\mathbf{F}^i_{\text{imag}} = \sum_{j=1, j\neq i}^{N} \frac{3\mu_0}{4\pi \mathbf{r}_{ji}^4} \left[\left(\mathbf{m}_j^{\mathrm{T}}\mathbf{m}_i - 5(\mathbf{m}_j^{\mathrm{T}}\hat{\mathbf{r}}_{ji})(\mathbf{m}_i^{\mathrm{T}}\hat{\mathbf{r}}_{ji})\right)\hat{\mathbf{r}}_{ji} + (\mathbf{m}_j^{\mathrm{T}}\hat{\mathbf{r}}_{ji})\mathbf{m}_i + (\mathbf{m}_i^{\mathrm{T}}\hat{\mathbf{r}}_{ji})\mathbf{m}_j\right], \qquad 4.$$

$$\boldsymbol{\tau}^i_{\text{imag}} = \sum_{j=1, j\neq i}^{N} Sk(\mathbf{m}_i)\mathbf{B}_{ji} = Sk(\mathbf{m}_i)\left[\frac{\mu_0}{4\pi ||\mathbf{r}_{ji}||^3}\left(3\hat{\mathbf{r}}_{ji}\hat{\mathbf{r}}_{ji}^{\mathrm{T}} - \mathbb{I}\right)\right]\mathbf{m}_j, \quad 5.$$

where $\hat{\mathbf{r}}_{ji}$ stands for the unit vector from the center of the jth microrobot to that of the ith, and $\mathbf{B}_{ji}$ is the magnetic field at the position of the ith microrobot generated by the jth microrobot. Typically, the global magnetic torque dominates the interactive torque, so that it can be assumed that all microrobots would always align with the global field—that is, the influence of $\boldsymbol{\tau}^i_{\text{imag}}$ is omitted (29, 30).

2.2. Fluidic Forces and Torques

Fluidic forces and torques are also important factors that determine a microrobot's motion. This subsection describes common fluidic forces and torques exerted on magnetic microrobots.

2.2.1. Fluidic drag force. The motion of a microrobot typically occurs in an incompressible fluid with laminar flow, and a hydrodynamic drag will be exerted on the microrobot. Generally, the fluidic drag force has the following expression:

$$\mathbf{F}_{\text{d}} = -\frac{1}{2}\rho A C_{\text{d}} ||\mathbf{v} - \mathbf{v}_{\text{f}}||^2 (\mathbf{v} - \mathbf{v}_{\text{f}}), \quad 6.$$

where $\mathbf{v}_{\text{f}}$, $\mathbf{v}$, and A are the fluid velocity, microrobot velocity, and frontal area of the microrobot, respectively. C_{d} is the Re-related drag coefficient, whose expression for intermediate Reynolds numbers is usually prescribed by an empirical expression (31). Loth (32) and Finn (33) gave the drag coefficients for a sphere and a cylinder moving in an infinite fluid field, respectively.

At the $Re \ll 1$ regime, $\mathbf{F}_{\text{d}}$ has a simplified expression. For spherical and cylindrical microrobots, the encountered drag forces can be expressed as Equations 7 and 8, respectively (32, 34):

$$\mathbf{F}^{\text{s}}_{\text{d}} = -\frac{3\pi d_{\text{s}}\mu}{\beta_{\text{s}}}(\mathbf{v} - \mathbf{v}_{\text{f}}), \quad 7.$$

$$\mathbf{F}^{\text{c}}_{\text{d}} = -\frac{3\pi d_{\text{c}}\mu}{\beta_{\text{c}}}\left(\bar{\mathbf{v}}_{\parallel} f_{E\parallel} + \bar{\mathbf{v}}_{\perp} f_{E\perp}\right), \quad 8.$$

where d_{s} and d_{c} are the effective diameters of the microrobots, and $\beta_{\text{s}}, \beta_{\text{c}} \geq 1$ are corrected weights considering the wall effect. In Equation 8, $\bar{\mathbf{v}}_{\parallel}$ and $\bar{\mathbf{v}}_{\perp}$ are the components of relative velocity that are parallel and perpendicular to the microrobot's symmetrical axis, respectively. $E = \frac{d_{\parallel}}{d_{\perp}}$ is the aspect ratio of the microrobot, and

$$d_{\text{c}} = d_{\parallel}E^{-2/3} = d_{\perp}E^{-1/3}, \quad 9.$$

$$f_{E\parallel} = \left(\frac{4}{5} + \frac{E}{5}\right)E^{-1/3} \text{ and } f_{E\perp} = \left(\frac{3}{5} + \frac{2E}{5}\right)E^{-1/3} \text{ for } 1 < E < 6. \quad 10.$$

The fluidic drag force ($Re \ll 1$) for other microrobot shapes can be approximated by Equation 7 or Equation 8.

2.2.2. Wall effect. The fluid flow near a boundary has a nonuniform distribution. For the smooth, infinite flat and cylindrical boundaries, the flow profile has approximately linear (35) and parabolic (36) profiles, respectively. Owing to this wall effect, when a microrobot moves close to a boundary, an extra retardation force is exerted on it (i.e., the drag force increases), and the closer

the microrobot is to the wall, the greater the wall effect is. Many numerical and experimental studies have revealed the empirical expression of the corrected drag force under the influence of the wall effect. These cases include a sphere rotating near a flat wall (37) and moving near a flat (35) or cylindrical (38) wall, a cylinder moving near a flat (39) or cylindrical (40) wall, and so on. On the other hand, the wall effect means that rotating microrobots are subject to unbalanced fluidic drag forces that result in translational locomotion near a boundary (41–43).

2.2.3. Fluidic vortex force. A rotating motion of microrobots generates fluidic vortices, which has been used to trap and manipulate microobjects (44–46). By utilizing the attractive long-range fluidic vortex force, one can aggregate a swarm of microrobots and control their locomotion as an entity (42, 47, 48). Although the aggregation process is difficult to formulate analytically, numerical simulations have successfully visualized and predicted the vortex-like swarm behaviors of magnetic microrobots (42, 47, 48). Another type of fluidic vortex force is the short-range vortex–vortex repulsive force (29). In a low-Reynolds-number regime, the expression of this force can be obtained by solving the Navier–Stokes equation (49).

2.2.4. Fluidic torque. The net fluidic torque is the cumulative result of fluidic forces exerted on a microrobot's body. For translational motion, this torque can be obtained via direct integration. For rotational motion, the fluidic torques for microrobots with axisymmetric bodies can be found in Reference 50.

2.2.5. Non-Newtonian fluids. Common fluids are Newtonian—that is, the viscosity distribution is invariant for a predefined working scenario. Given that many biological fluids are non-Newtonian viscoelastic fluids (e.g., mucus and vitreous humor), it is meaningful to study microrobot motion in non-Newtonian fluids (15, 16). For simplified cases, non-Newtonian fluids can be modeled as generalized Newtonian fluids whose viscosity is proportional to the nth power of the shear rate: $\mu = K\dot{\gamma}^n$ ($n \neq 0$). Utilizing this property, Qiu et al. (51) were able to formulate new motion principles for cases other than traditional nonreciprocal motion, which represents important progress toward biomedical applications using magnetic microrobots.

2.3. Boundary Forces

The motion of many magnetic microrobots relies on boundary forces, that is, contact forces exerted by boundaries. Stick–slip motion (52–54) requires a friction force to maintain stable translational motion, which can be provided by the boundary supporting force that results from the apparent weight of the microrobot (53), the electrostatic force between the boundary and the microrobot (55), and so on. Specifically, sophisticated electrostatic (56) and electromagnetic (57) gridding substrates have been designed to selectively anchor and actuate individual magnetic microrobots, respectively. Moreover, lateral boundary contact can be utilized to selectively counteract the magnetic forces in order to independently control the motions of multiple magnetic microrobots (58) or the statistical parameters of a swarm of particles (59).

3. MOTION PRINCIPLES OF INDIVIDUAL MAGNETIC MICROROBOTS

Motion control of individual magnetic microrobots has been widely studied and demonstrated, and the fundamentals have been well established. Here, we review several classic controllable motion modalities (shown in **Figure 1**), with an emphasis on their control principles. **Table 1** provides a visualization of forces and torques related to these motion modalities.

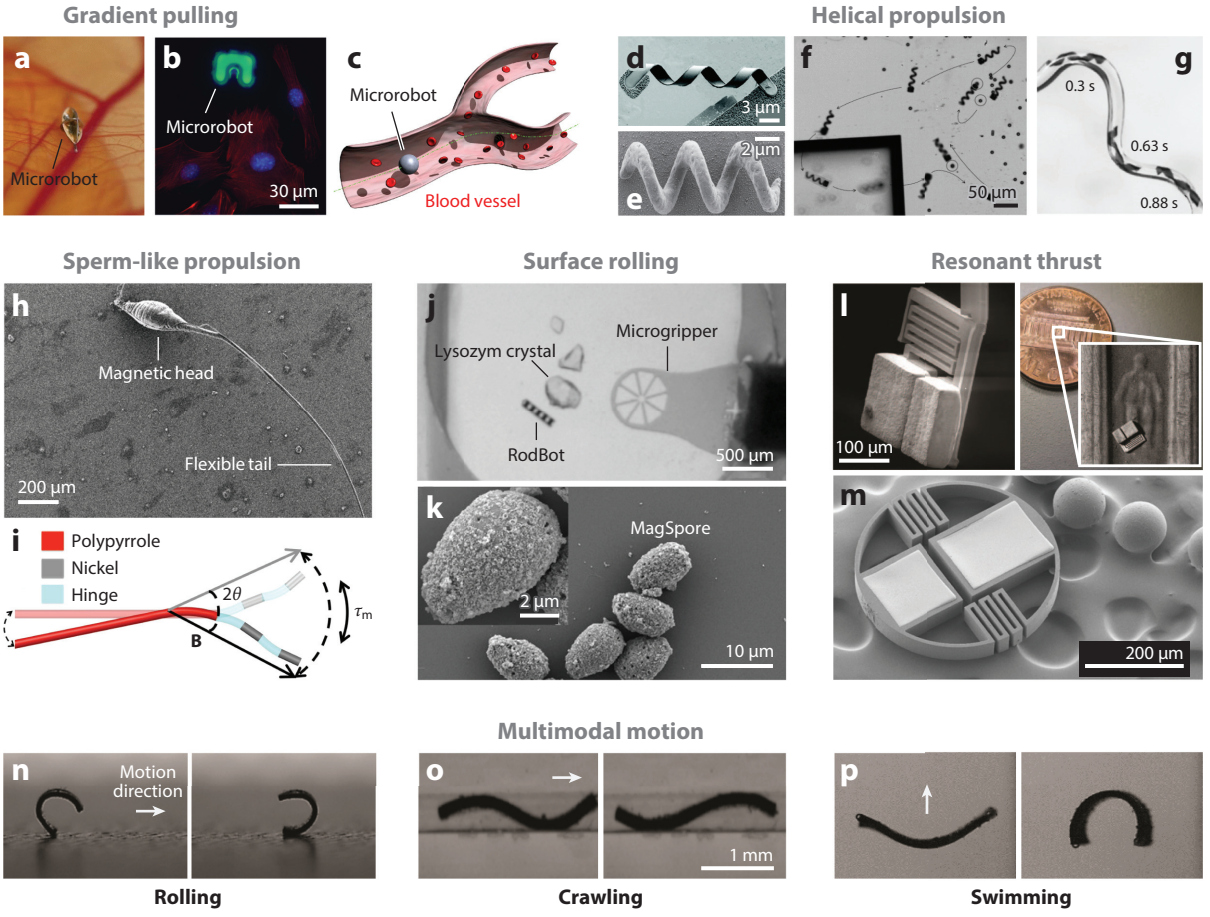

Figure 1

Representative examples of controllable locomotion of individual magnetic microrobots. (*Top left*) Gradient pulling. (*a*) A magnetic microrobot controlled and docked to a blood vessel as a proposed therapy for retinal vein occlusions. Panel adapted from Reference 60 with permission from IEEE. (*b*) A fluorescence-imaging-tracked magnetic microrobot being used for cell manipulation. Panel adapted from Reference 54 with permission from SAGE Publishing. (*c*) A spherical magnetic microrobot controlled in a blood vessel along a reference trajectory. Panel adapted from Reference 61 with permission from IEEE. (*Top right*) Helical propulsion. (*d*) A helical microrobot with self-scrolled thin film ribbons as the tail and thin metal films as the soft-magnetic head. Panel adapted from Reference 62 with permission from AIP Publishing. (*e*) Direct laser writing of biocompatible helical microrobots coated with iron. Panel adapted from Reference 63 with permission from RSC Publishing. (*f*) Cargo transport using a helical microrobot. Panel adapted from Reference 64 with permission from Wiley. (*g*) A soft helical microrobot swimming through a curved conduit. Panel adapted from Reference 65 with permission from Science Publishing Group. (*Middle left*) Sperm-like propulsion. (*h*) Soft robotic sperm fabricated by electrospinning. Panel adapted from Reference 66 with permission from IEEE. (*i*) A magnetic multilink nanorobot with undulatory locomotion. Panel adapted from Reference 67 with permission from ACS Publishing. (*Middle center*) Surface rolling. (*j*) The rolling RodBot for crystal harvesting. Panel adapted from Reference 44 with permission from IEEE. (*k*) The rolling MagSpore for toxin sensing. Panel adapted from Reference 13 with permission from Science Publishing Group. (*Middle right*) Resonant thrust. (*l*) Scanning electron microscopy image of a MagMite. Panel adapted from Reference 55 with permission from SAGE Publishing. (*m*) Scanning electron microscopy image of the PolyMite, with polystyrene beads approximately 120 μm in diameter. Panel adapted from Reference 68 with permission from IEEE. (*Bottom*) Multimodal motion of a soft microrobot, showing (*n*) rolling, (*o*), crawling, and (*p*) swimming. Panels adapted from Reference 69 with permission from Nature Publishing Group.

Table 1 Torques/forces related to the motion principles of individual magnetic microrobots and their extension to multiagent or swarm control

		Gradient pulling	Helical propulsion	Sperm-like propulsion	Surface rolling	Resonant thrust
Motion dimension		2D/3D	2D/3D	2D/3D	2D	2D
Global magnetic force[a]		✓ ★	✓	✓	✓	✓
Global magnetic torque[a]		✓	✓	✓	✓	✓
Interactive magnetic force[a]		☆	☆		★	✓
Fluidic drag force[a]		✓	✓	✓	✓	✓
Wall effect[a]		✓	✓	✓	✓	✓
Fluidic vortex force[a]		☆	★		★	
Boundary forces[a]		✓ ☆ ★	✓	✓	✓	✓
Field inhomogeneity[b]		☆	☆			
Property asymmetry[b]		☆	☆	☆		☆
References	Individual	52, 54, 61, 70–72	62–65, 73, 74	66, 67, 75–77	13, 43, 78–81	55, 68
	Multiagent	29, 53, 56–58, 82–88	89–95	96		97
	Swarm	59, 98, 99	100		34, 42, 48, 101–103	

Symbols: ✓, essential torque/force of the motion of an individual microrobot; ✓, nonessential and nonignorable torque/force that may be exerted on an individual magnetic microrobot; ☆, specific torque/force or strategy that has been used to trigger multiagent control; ★, specific torque/force or strategy that has been used to trigger swarm control.

[a]Section 2 provides detailed explanations of these terms.

[b]Section 4 provides detailed explanations of these terms.

3.1. Gradient Pulling

As indicated by Equation 2, magnetic fields with gradients can drive a magnetic microrobot to move via a pulling force, $\mathbf{F}_{\text{gmag}}$. Pure gradient pulling is one of the simplest motion modalities of magnetic microrobots: The motion control of a magnetic microbead requires only the adjustment of the gradient strength and direction (61, 70, 71). A stable moving velocity is reached when

$$\mathbf{F}_{\text{gmag}} = -\mathbf{F}_{\text{d}}. \qquad 11.$$

Interestingly, by designing and controlling a locally convergent gradient field, one can induce flagellated magnetotactic bacteria to gather together as a swarm and perform navigated motion and manipulation tasks (98, 99).

For more complex cases, the combination of in-plane gradient pulling and out-of-plane oscillating fields achieves stick–slip motion (52–54). One can control the motion direction via the yaw angle of the gradient field, and the moving velocity is sensitive to the waveform and frequency of the oscillating field and the strength of the gradient field (52). The relationships are usually obtained through characterization, and these field parameters can serve as control inputs for velocity control. Simultaneously controlling the orientation and motion direction of nonspherical magnetic microrobots requires stationary electromagnetic systems with at least eight coils (26). Kummer et al. (72) described field and gradient control methods in detail. Note that six-degree-of-freedom magnetic motion control also requires a particular microrobot design (104). **Table 1** lists some strategies that can extend the gradient-pulling motion of individual microrobots to multiagent control or swarm control, the details of which are given in Section 4.

3.2. Helical Propulsion

In a low-Reynolds-number environment, some bacteria (e.g., *Caulobacter crescentus*) swim using a helical propulsion mechanism (105). Inspired by nature, many magnetic helical microrobots have been fabricated for micromanipulation and delivery purposes (62–64, 73). Soft-bodied helical microrobots have better environmental adaptability due to their shape deformation capability (65). The propulsion motion along the major axis of a helical microrobot is described by (106)

$$\begin{bmatrix} f_{\text{hm}} \\ \tau_{\text{hm}} \end{bmatrix} = \begin{bmatrix} a & b \\ b & c \end{bmatrix} \begin{bmatrix} v_{\text{hm}} \\ \omega_{\text{hm}} \end{bmatrix}, \tag{12.}$$

which linearly relates the propulsion velocity v_{hm} and angular velocity ω_{hm} with the nonfluidic applied force f_{hm} and nonfluidic applied torque τ_{hm} via four principal quantities. The nonfluidic applied forces are gravity, buoyancy, friction, and magnetic forces; the only nonfluidic torque is the magnetic torque (74). From a motion control perspective, Equation 12 can be rearranged with the nonfluidic applied force f_{hm} and angular velocity ω_{hm} as the input variables (25):

$$\begin{bmatrix} v_{\text{hm}} \\ \tau_{\text{hm}} \end{bmatrix} = \begin{bmatrix} 1/a & -b/a \\ b/a & c - b^2/a \end{bmatrix} \begin{bmatrix} f_{\text{hm}} \\ \omega_{\text{hm}} \end{bmatrix}. \tag{13.}$$

3.3. Sperm-Like Propulsion

The locomotion of sperm cells is achieved by periodically changing their tail morphology in a nonreciprocal manner. By decorating the sperm cells with magnetically driven parts, one can remotely control their motion using magnetic fields (75, 76). To mimic the efficient sperm-like propulsion, artificial sperms are fabricated that usually consist of a magnetic head and a long elastic tail (66, 67, 107). A constant-strength oscillating magnetic field with sinusoidally varying orthogonal components induces a bending wave along the tail, and the tail deformation is governed by (77)

$$\kappa \frac{\partial^4}{\partial x^4} y(x,t) + c_{\text{n}} \frac{\partial}{\partial x} y(x,t) = 0, \tag{14.}$$

where $y(x, t)$ is the deformation of the flexible tail with a bending stiffness of κ, relative to the coordinate frame of the magnetic sperm $\{\text{O} - \mathbf{xy}\}$. Here, $\mathbf{x}$ and $\mathbf{y}$ are orthonormal vectors such that $\mathbf{x}$ is oriented along the long axis of the sperm, and O locates at the center of the sperm head. c_{n} and c_{t} are normal and tangential drag coefficients. By solving Equation 14, whose boundary conditions are shown in Reference 77, one can simultaneously obtain the motion dynamics of the magnetic sperm in free static fluid:

$$\int_0^L \frac{(c_{\text{n}} - c_{\text{t}}) v_y \frac{\text{dy}}{\text{dx}} - v_x \left(c_{\text{t}} + c_{\text{n}} \left(\frac{\text{dy}}{\text{dx}} \right)^2 \right)}{1 + \left(\frac{\text{dy}}{\text{dx}} \right)^2} \text{dx} = 3\pi d_{\text{sh}} \mu v_x, \tag{15.}$$

where L and d_{sh} are the tail length and head diameter of the magnetic sperm, respectively. The quantitative relationship between the motion velocity (v_x) and field frequency (control input) is calibrated through simulations and experimental characterizations. Different tail parameters lead to varied swimming characteristics, which can be utilized to realize multiagent control (96).

3.4. Surface Rolling

As another type of efficient magnetic torque-driven motion, rolling microrobots have many applications, such as mobile sensing (13, 43) and micromanipulation (78, 80). This type of motion

relies on the wall effect introduced in Section 2.2.2, and the motion dynamics is described by (79)

$$\begin{cases} v_x = a_0\omega(t)\cos(\alpha(t)) + D_x(t) \\ v_y = a_0\omega(t)\sin(\alpha(t)) + D_y(t) \end{cases}, \qquad 16.$$

where a_0 is a positive constant, and $D_x(t)$ and $D_y(t)$ are the generalized disturbances of the x and y directions, respectively. One can control the motion direction and motion velocity by adjusting the yaw angle α and frequency ω of the rotating magnetic field. The vortex force can be utilized to extend this type of motion to swarm control, as discussed in Section 4.

3.5. Resonant Thrust

Resonant actuators absorb large amounts of energy from the driving signal when the frequency of the signal closely matches a natural resonant frequency of the actuator structure. When the absorbed elastic energy is released, a thrust force can be generated for locomotion. Frutiger et al. (55) proposed the MagMite (shown in **Figure 1*l***), which consists mainly of two heavy parts with paramagnetic material and a connecting spring part. After being magnetized by an externally applied magnetic field, the magnetic parts are pulled together by the induced magnetic gradient. When the field is removed, the energy stored in the spring then pushes them apart. The energy transformation efficiency reaches its maximum when the field frequency equals the resonant frequency of the structure, calculated as

$$\omega_r = \frac{1}{2\pi}\sqrt{\frac{k}{m} - \frac{c^2}{4m^2}}, \qquad 17.$$

where m and c are the mass and the damping coefficient of the oscillating heavy part, respectively, and k is the spring constant. To break the symmetrical oscillation that would cause in-place vibration motion, an additional boundary force mentioned in Section 2.3 is applied. With the same principle, Tung et al. (68) designed the PolyMite, which contains two symmetric springs so that the locomotion is more stable in the lateral direction. The control inputs of this type of locomotion are the field strength and yaw angle, which control the motion velocity and direction, respectively. Different resonant frequencies can be obtained by using different structural designs, which can then be used for multiagent control, as shown in Reference 97.

3.6. Multimodal Motion

The above-mentioned motion modalities are often individually selected for magnetic microrobots, which could restrict their motion adaptability when working in varying environments. For example, the fluid viscosity and substrate properties may change, and the motion dimension may be required to switch between 2D and 3D. To this end, recent progress in soft microrobots makes multimodal motion possible (69). The high mobility enables up to eight types of motion, such as 2D rolling, 2D crawling, and 3D swimming, as shown in **Figure 1*n–p***. The combination of motion modalities broadens the capability of magnetic microrobots and enhances the application possibilities.

4. MULTIAGENT AND SWARM CONTROL OF MAGNETIC MICROROBOTS

In contrast to robots at larger scales (108), it is difficult to equip microrobots with onboard sensors and actuators for individual motion feedback and control, which leads to challenges in the

motion control of multiple microrobots and large swarms (on the order of hundreds to millions of microrobots). For magnetic microrobots, specific challenges originate from the fact that all the controlled agents receive the same control inputs (109). A time line of representative developments for multiagent and swarm control is depicted in **Figure 2**.

4.1. Multiagent Control

As with individual microrobot control, multiagent control of magnetic microrobots ignores interactive forces in most cases unless some magnetic microrobots work in close proximity to each other. Therefore, classic individual motion principles can be extended to multiagent control, as summarized in **Table 1**. The most commonly reported multiagent control strategies fall into four categories: breaking the property symmetry of magnetic microrobots, utilizing the inhomogeneity of magnetic fields, creating specialized boundaries, and controlling the interaction forces.

4.1.1. Breaking the property symmetry of magnetic microrobots. Property differences among magnetic microrobots can cause them to behave differently in response to the same control input. Therefore, breaking the property symmetry enables the same control input to control the motion of multiple microrobots independently (114).

Different velocity responses to a field frequency may be created by varying the structural parameters. Kratochvil et al. (97) fabricated two resonant microrobots with different eigenmodes, which caused the two microrobots to have different resonant responses. Khalil et al. (96) fabricated sperm-like microrobots with nonidentical tails to obtain different frequency–velocity responses. Geometrically and magnetically identical helical microrobots (also called artificial bacterial flagella) could have different step-out frequencies after a modification of their surface chemistries, which changes their interactions with fluid (89). Different motion direction responses to field torque may also be created. Becker et al. (87) showed that, by exploring the inhomogeneity of the tuning model, one can steer multiple *Tetrahymena pyriformis* cells to independent goals.

The other property that frequently serves as the triggering variable in multiagent control is the magnetization. Mandal et al. (115) demonstrated that, when microrobots with the same geometrical properties have different directions of permanent magnetization with respect to their body axis, they move in different directions under the same oscillating magnetic fields, but when they are subject to rotating fields, they move in the same direction. Other studies have used magnetic microrobots with similar geometrical properties but different magnetization strengths or materials to independently control the motion of multiple microrobots (82, 90). By combining the geometrical and magnetization differences, Diller et al. (83) designed several microrobots and implemented independent 3D control of multiple magnetic microrobots. As a special case, the property of magnetization profiles can also be utilized to create distinct field responses under the same field (91).

This type of method requires only a global magnetic field, so the field control is simple. However, it relies on the precise fabrication and modeling of microrobots with different magnetic responses. At the microscale, the batch fabrication of microrobots with varying elaborate structures and magnetization properties is difficult.

4.1.2. Utilizing the inhomogeneity of magnetic fields. With various custom magnetic manipulation systems being developed, control strategies utilizing inhomogeneous magnetic fields have been proposed to control multiple magnetic microrobots. As the simplest case, a single magnet dipole source has the ability to generate two rotating magnetic fields with arbitrary independent rotation axes at any two points so that two helical microrobots can be independently

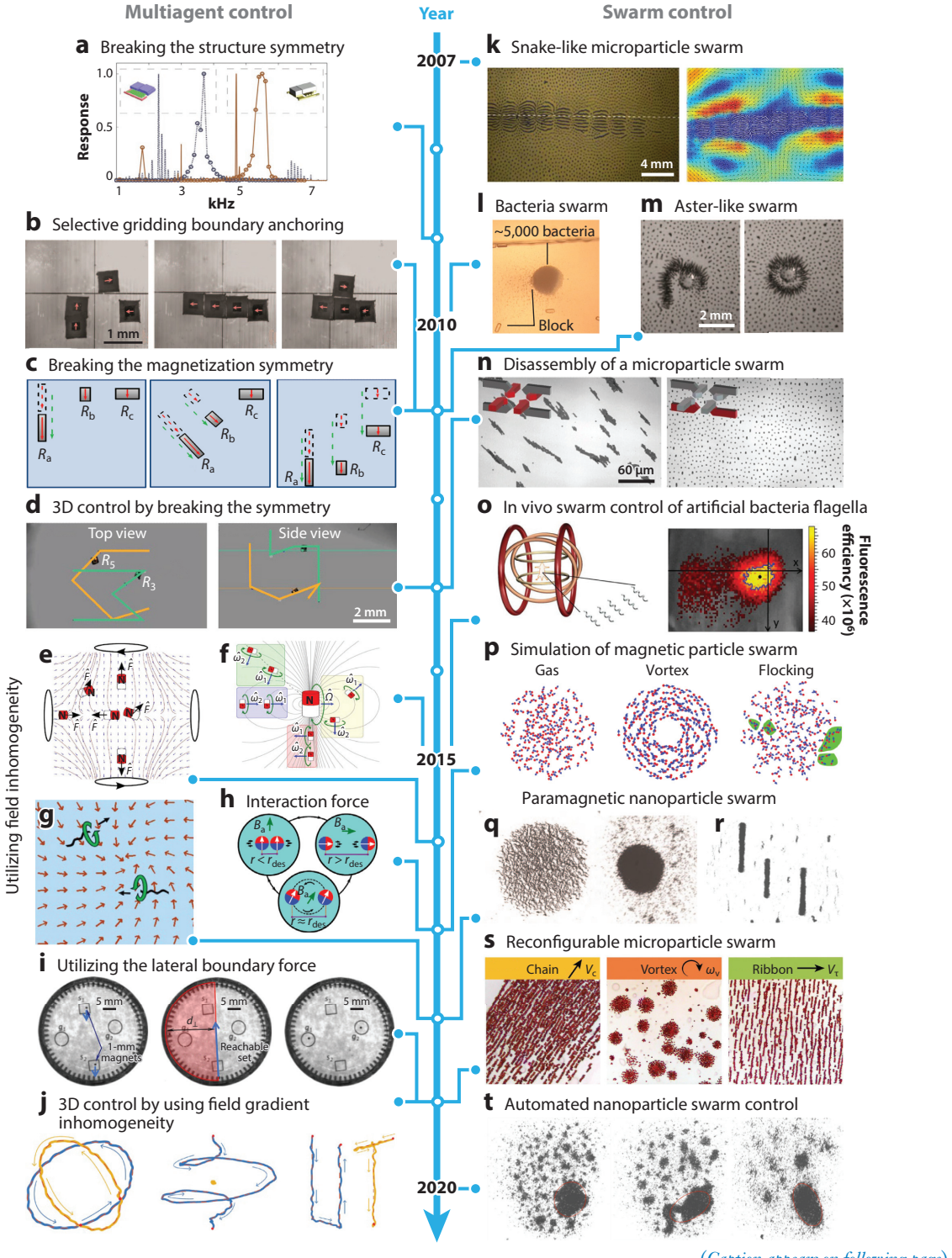

(*Caption appears on following page*)

Figure 2 (*Figure appears on preceding page*)

Time line of representative developments for multiagent and swarm control of magnetic microrobots. (*Left*) Multiagent control. (*a*) Resonant microrobots with different structures. Panel adapted from Reference 97 with permission from IEEE. (*b*) Assembly and disassembly of multiple microrobots controlled using an electrostatic anchoring surface. Panel adapted from Reference 56 with permission from IEEE. (*c*) Independent control of multiple microrobots with different magnetization strengths or materials. Panel adapted from Reference 82 with permission from SAGE Publishing. (*d*) Independent control of multiple magnetic microrobots in 3D by breaking the property symmetry. Panel adapted from Reference 83 with permission from SAGE Publishing. (*e–g*) Independent multiagent control through field inhomogeneity. Microrobots are driven by magnetic force (panel *e*) or torque (panels *f* and *g*), and magnetic fields are generated by a single magnet (panel *f*) or multiple electromagnets (panels *e* and *g*). Panels adapted from References 84, 93, and 92, respectively, with permission from IEEE. (*h*) Two-agent formation control of magnetic microrobots by utilizing the magnetic interactive force. Panel adapted from Reference 29 with permission from Springer Publishing. (*i*) Two-agent independent control by utilizing the lateral boundary force. Panel adapted from Reference 58 with permission from IEEE. (*j*) Independent 3D control of two magnetic microrobots by utilizing field gradient inhomogeneity. Panel adapted from Reference 86 with permission from IEEE. (*Right*) Swarm control. (*k*) A snake-like microparticle swarm on the fluid–air interface. Panel adapted from Reference 110 with permission from APS Publishing. (*l*) A swarm of magnetotactic bacteria. Panel adapted from Reference 98 with permission from IEEE. (*m*) An aster-like microparticle swarm. Panel adapted from Reference 111 with permission from Nature Publishing Group. (*n*) Disassembly control of a microparticle swarm. Panel adapted from Reference 103 with permission from RSC Publishing. (*o*) In vivo swimming of a swarm of artificial bacterial flagella. Panel adapted from Reference 17 with permission from Wiley. (*p*) Discrete particle simulations to reveal swarm behaviors. Panel adapted from Reference 47 with permission from Science Publishing Group. (*q*) A vortex-like paramagnetic nanoparticle swarm. Panel adapted from Reference 42 with permission from SAGE Publishing. (*r*) Ribbon-like paramagnetic nanoparticle swarms. Panel adapted from Reference 112 with permission from Nature Publishing Group. (*s*) A reconfigurable magnetic microparticle swarm. Panel adapted from Reference 48 with permission from Science Publishing Group. (*t*) Automated nanoparticle swarm control based on statistics. Panel adapted from Reference 113 with permission from IEEE.

controlled (93). Magnetic manipulation systems with multiple electromagnetic coils are more commonly used. By solving their system actuation equations, one can generate spatially selective fields (92, 94) or gradients (84, 85) based on the superposition law to obtain independent multiagent control. Recently, Ongaro et al. (86) developed a nine-coil system and obtained independent 3D control of two identical or nonidentical gradient-pulling microrobots.

This type of method has more application potential because it does not depend on precise microrobot fabrication and modeling, and it allows for independent control over both identical and nonidentical microrobots. On the other hand, existing techniques have shown accurate modeling results of field distributions for both permanent magnets and electromagnetic coils. The main concern is that, for multiple-coil systems without analytical coil field models, the proper solution would require solving a nonconvex optimization problem, which involves significant computational effort, especially as the number of coils increases.

4.1.3. Creating specialized boundaries. Specialized boundaries capable of providing localized boundary forces can be created to break the symmetry of actuation forces among multiple microrobots under excitation by the same field signals. Sophisticated substrates with independently controllable grids have been designed to selectively anchor individual microrobots by controlling the electrostatic force (56) or to independently actuate individual microrobots by controlling the electromagnetic force (57). Both approaches can provide independent motion control on 2D substrates. As a special strategy, lateral nonslip boundaries serve as static obstacles to constrain the motion of particles (58), and by designing control algorithms, one can independently control the positions of two particles.

Since gridding substrates fully decouple the control inputs on individual magnetic microrobots, they are suitable for complex assembly and micromanipulation tasks. In addition, the substrates could offer very high control frequencies and good motion control robustness. However, this type of method only allows microrobots to work near a substrate or lateral boundaries, which makes an

extension to 3D applications difficult. The substrates and lateral boundaries also have strict and even hard-to-satisfy requirements for real applications.

4.1.4. Controlling the interaction forces. The above-mentioned multiagent control methods ignore the interactive forces among microrobots (95). In fact, when multiple magnetic microrobots work in close proximity to each other, the interactive magnetic force expressed by Equation 4 should be taken into consideration. As shown by Salehizadeh & Diller (29), by modeling the relationship between the magnetic interaction states and the agent heading angles, one can regulate the interagent spacing, heading, and position of two magnetic microrobots on an oil–water interface. Moreover, the hydrodynamic vortex force generated by rotating microrobots can also be utilized. On an air–fluid interface, when the force balance between the repulsive short-range vortex interaction force and the attractive magnetic interaction force is reached, the pattern of multiple agents becomes stable (30, 88). The distance between two agents is tuned by controlling the agents' field rotation frequency and magnetic orientation, which influence the interactive hydrodynamic force and the average interactive magnetic force, respectively. This type of method provides a solution for multiple magnetic microrobots that work close to each other, but extending the theories to 3D environments is difficult, and the problem has yet to be solved.

4.2. Swarm Control

Swarm behaviors are common in nature, with examples ranging from animals and insects to bacteria, and these behaviors are often significant for biological living or survival. Controlling swarms on the order of hundreds to thousands or even millions of robots is one of the primary challenges in magnetic microrobotics. Owing to the small size of the robots and the large population of a swarm, the multiagent control methods discussed in Sections 4.1.1 and 4.1.2 lose effectiveness, but swarm control of magnetic microrobots using global magnetic field is favorable (116). In addition, magnetic microrobots that can be batch fabricated via microfabrication technologies (e.g., magnetic micro- or nanoparticles) are preferable for swarm control. Moreover, in contrast to individual and multiagent control, a unique feature of swarm control is that the interactive force should never be ignored. This feature dramatically increases the difficulty of the theoretical modeling of swarm behaviors. As a result, simulation becomes a powerful tool for swarm control of magnetic microrobots.

4.2.1. Swarm pattern formation via dynamic assembly. Under the excitation of external global dynamic magnetic fields, complex dynamic magnetic and fluidic interactive forces can be induced in a swarm of magnetic microrobots. Governed by these forces, dynamic assembly processes occur and stable swarm patterns can be formed after force equilibria are reached, such as snake-like (110), ring-like (102), aster-like (111), vortex-like (42), and ribbon-like (112) patterns. For the formation mechanism, the dynamic assembly is generally activated by a global periodic magnetic field that induces the synchronizing magnetic torque-driven motion of each unit in the swarm. Then, generated by the synchronizing motion, the regular fluid flow and directional average magnetic interactive force over an actuation period create the driving force for the assembly process until a force-equilibrium state is reached, which may correspond to a stable swarm pattern. Because of the multiple interaction forces and stochastic motion of micro- and nanoparticles, analytical solutions of assembly processes are difficult to obtain, and thus simulation approaches are usually adopted (42, 47, 48).

The stable swarm patterns are related mainly to the field waveform and working environment. For example, although the same alternating field waveforms are applied to the same magnetic

microparticle swarm, the resulting swarm patterns are completely different for a swarm located at an air–fluid interface (110) and a swarm at a silicon oil–Na_2SO_4 solution interface (111). Simulation and experimental analysis have shown that the generated flow is the dominating factor. The field waveform, as the motion excitation source, plays the most important role in determining the swarm pattern. Yu et al. demonstrated that, for the same magnetic nanoparticle swarm distributed on a flat substrate, rotating fields and oscillating fields induce a vortex-like swarm pattern (42) and a ribbon-like swarm pattern (112), respectively. The dynamic assembly of the former is dominated by the long-range attractive vortex force, while that of the latter is dominated by magnetic attractive force. The conical fields used by Yan et al. (117) and Mohoric et al. (118) even generate 3D tube and hollow cylinder patterns, which, however, are a precursor to structural instability.

In addition to swarm pattern generation, field parameters can be controlled to tune the equilibrium state of the swarm pattern. Different combinations of the frequency and opening angle of conical fields lead to different 3D or 2D pattern phases, as shown by Yan et al. (117) and Mohorich et al. (118). Pattern phases can even be directly switched from one to another by changing the global field waveform (48). This reconfigurable magnetic microrobot swarm (48) has four distinct swarm pattern phases that correspond to four magnetic field waveforms. The shape of a given swarm pattern can also be controlled by adjusting field parameters. The shape ratio of the ribbon-like nanoparticle swarm (112) and the area of the vortex-like nanoparticle swarm (42) are tuned by the field ratio of the oscillating field at the x–y plane and the field frequency of the in-plane rotating field, respectively.

The size of a magnetic micro- or nanoparticle has little influence on the form of swarm patterns, because each particle is approximately equivalent to a magnetic dipole, and particles of different shapes and sizes generate similar fluid flows if the other conditions are the same. For example, rotating magnetic fields induce circular vortex-like patterns for many types of spherical particle with a wide range of diameters: hundreds of nanometers (42), several micrometers (101, 118, 119), tens of micrometers (47), or hundreds of micrometers (120). The same principle of swarm pattern formation also applies to peanut-shaped (48) and helix-shaped (100) magnetic microrobots, which indicates that the microrobot shape may not be a significant factor in pattern formation.

Furthermore, for some applications, a reversible disassembly process is necessary to make the microrobot swarm cover a desired region or create the desired density for localized delivery or therapy—for example, for the treatment of local hyperthermia (121). To this end, control of the distribution region or density of the microrobot swarm is the key technology. Some methods have been recently proposed for swarm disassembly (34, 103, 122).

As a special case, beyond the swarm pattern formation determined by dynamic magnetic and fluidic forces, an array of small permanent magnets provides a strong localized gradient field that dominates the assembly process (123). Each magnet determines the motion of nearby microrobots, so that particular patterns can be achieved by programming the magnet distribution. However, the major drawback is that the magnet array cannot be dynamically programmed.

4.2.2. Swarms without a stable pattern. Unlike the dynamically assembled swarm patterns described in Section 4.2.1, which are governed by global or local regular fluid flows, some magnetic microrobot swarms do not form stable patterns. Instead, all the agents in the swarm have an identical motion under the actuation of a global magnetic field and can move in pace with each other. Examples include helical microrobots, surface-rolling microrobots, and gradient-pulling microrobots. A swarm of helical microrobots can swim in the intraperitoneal cavity of a BALB/c mouse (17) and in the vitreous body of an eye (15). Since there are no strong forces keeping the swarm together, if it is subject to disturbances, the swarm shape can easily change, and some parts of the swarm can even be lost. This phenomenon also occurs for swarms of surface-rolling microparticles

moving on substrates with obstacles (124) or curved channels (125). Driven by a global magnetic gradient field, a swarm of gradient-pulling microrobots will move together along the gradient direction (126). In particular, gradient-guided flagellated magnetotactic bacteria can be gathered together by applying a focusing magnetic gradient field (98). Thanks to the self-propulsion property of the magnetotactic bacteria, they are capable of generating 3D bacteria swarms (127), and this property enables them to aggregate together.

4.2.3. Swarm motion control as an entity. The motion of a swarm of magnetic microrobots is controlled by a small number of magnetic inputs. From the motion control perspective, this is an underactuated system because each microrobot cannot be individually actuated and controlled. Therefore, the literature has commonly treated the entire swarm as an entity. This is a feasible strategy for swarms that can form stable patterns, the motion of which is robust to external force and disturbances (42, 48, 110–112). Using the strong ensemble force, these swarms can even trap and transport cargoes (42, 48, 111). By comparison, loss of individual components during motion is common for magnetic microrobot swarms without stable patterns (17, 124, 125). Therefore, microrobot swarms with stable patterns have higher microrobot utilization ratios and higher delivery efficiency than those without stable patterns. However, most swarm pattern formations rely on a substrate or 2D interface, which limits their application scenarios.

5. CLOSED-LOOP MOTION CONTROL OF MAGNETIC MICROROBOTS

With established principles of magnetic microrobot motion, closed-loop control is required to improve the accuracy and efficiency for microrobotic tasks (e.g., delivery and micromanipulation). From individual and multiagent to swarm magnetic microrobots, closed-loop control is designed and implemented to ensure high-accuracy motion and accomplish microrobotic tasks automatically. The general structure of closed-loop motion control systems for magnetic microrobots is depicted in **Figure 3**. To date, the mainstream research focus has been on the development of the motion controller, magnetic manipulation system, feedback instrument, and signal-processing methods, and the majority of works have used a preset trajectory or manual inputs to replace the motion planning function or adopt mature static planning methods. However, for complex and dynamic working environments, advanced motion planning methods need to be further taken into consideration.

Since magnetic manipulation systems have been thoroughly reviewed by Abbott et al. (18), here we describe how the four other parts are applied in magnetic microrobotics and critically review and discuss state-of-the-art works. Representative results of these studies are illustrated in **Figure 4**.

5.1. Motion Planning and Controller

When a task is given, motion planning is responsible for generating feasible or even optimal targeted motion for the microrobot, i.e., $\mathbf{q}^*(t)$, which is composed of a series of future targeted states of the microrobot, i.e., $\mathbf{s}^*(t)$. Based on the obtained information about the environment and current state of the microrobot, many traditional planning algorithms can be readily adopted or improved for use. For example, search-based algorithms, such as A* (80) and rapidly exploring random trees (RRT) (130), have been used for global path planning for individual microrobots. To further improve the planning optimality, iteration-based algorithms are applied, such as particle swarm optimization (81) for path generation and the genetic algorithm (131) for swarm pattern

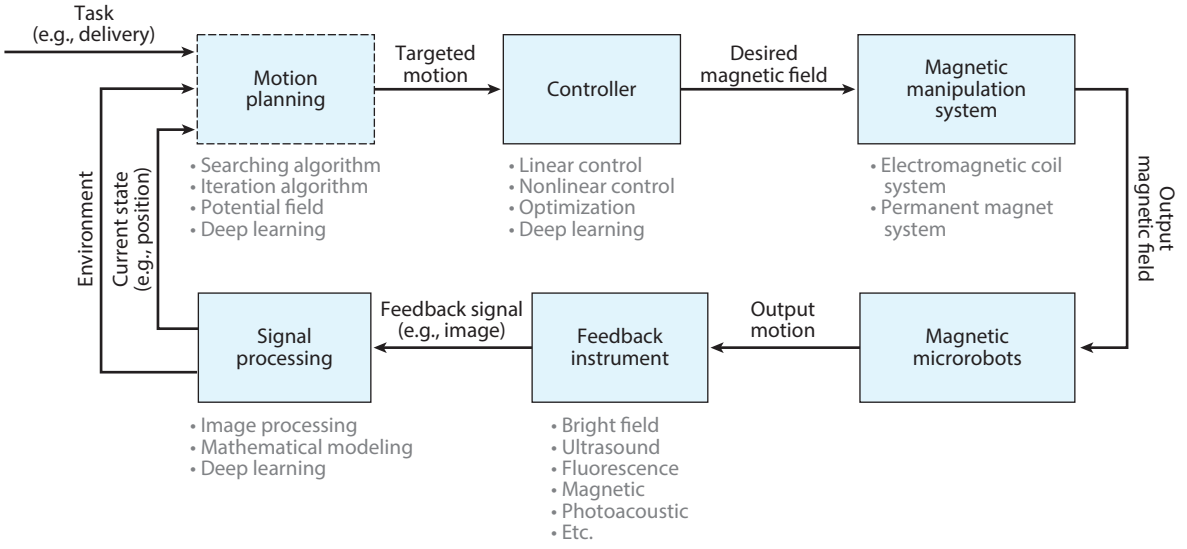

Figure 3

The general structure of closed-loop motion control systems for magnetic microrobots, which comprises five main parts: motion planning, a controller, a magnetic manipulation system, a feedback instrument, and signal processing. When a given task is accomplished, the motion planning part will stop the motion control loop.

generation. However, due to the limited computational efficiency, these two types of methods are adequate only for static environments. As a solution for dynamic planning, recent studies have designed potential field-based algorithms. By using dynamic-avoidance vectors, Kim et al. (132) and Li et al. (133) were able to perform dynamic microrobot navigation even within in vivo environments. One potential direction for dynamic planning in more complex environments is the deep learning–based methods that have already been applied for autonomous vehicles. Another unsettled issue in planning for multiagent and swarm microrobotics is that the targeted motion is preset or manually set in almost all current works (83, 85, 86, 113, 127). For magnetic microrobot swarms, in addition to the path planning, pattern formation (131) and deformation planning (134) are vital for optimal swarm generation and environmental adaptability, respectively.

The controller performs the core task of accurate, automated motion control, the goal of which is to generate control inputs $\mathbf{u}(t)$ so that the output motion will make the future state of the microrobot $\mathbf{s}(t)$ converge to its desired value $\mathbf{s}^*(t)$ obtained by motion planning, i.e.,

$$\mathbf{s}^*(t) - \mathbf{s}(t) \xrightarrow{\mathbf{u}(t)} 0, \text{ when } t \to \infty. \qquad 18.$$

After approximately 20 years of development, the fundamentals of automated individual control have been solidly established. Conventional proportional–integral–derivative (PID) control is the simplest controller that fulfills Equation 18, as shown in many works in the literature (54, 79, 129, 135–137). Simple PID (or part of PID) control is also adopted in multiagent control for preliminary validation of the independent control theory (29, 83, 84). To implement the derivative control action and eliminate feedback noise, position and velocity observers should be utilized (86). Since PID control is a linear method that does not take into account the nonlinearities of the motion dynamics (e.g., the wall effect) or nonlinear uncertainties caused by the inaccurate modeling of the motion dynamics and electromagnetic system, deficiencies in the tracking performance are obvious, as shown in the corresponding results in **Figure 4**.

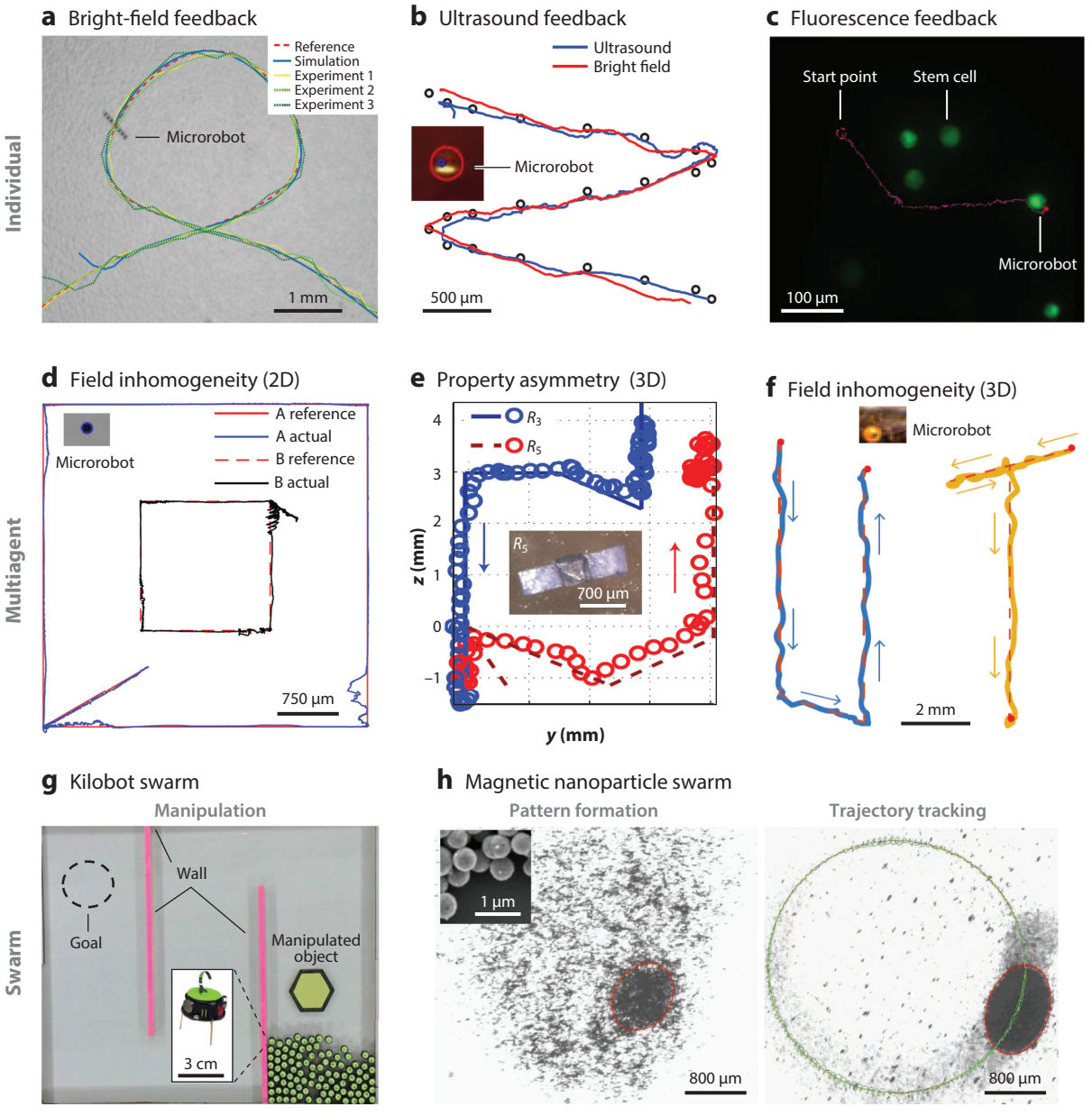

Figure 4

Representative closed-loop control results for magnetic microrobots. (*Top*) Results for individual microrobots. (*a*) Control of a rolling microrobot under bright-field feedback. Panel adapted from Reference 128 with permission from IEEE. (*b*) Control of a gradient-pulling microrobot under ultrasound feedback. Panel adapted from Reference 129 with permission from IEEE. (*c*) Control of a surface-rolling microrobot under fluorescence feedback. Panel adapted from Reference 81 with permission from IEEE. (*Middle*) Results for multiple microrobots. (*d*) 2D control of two gradient-pulling microrobots by using field inhomogeneity. Panel adapted from Reference 85 with permission from IEEE. (*e*) 3D control of two gradient-pulling microrobots by using property asymmetry. Panel adapted from Reference 83 with permission from SAGE Publishing. (*f*) 3D control of two gradient-pulling microrobots by using field inhomogeneity. Panel adapted from Reference 86 with permission from IEEE. (*Bottom*) Results for swarms of microrobots. (*g*) Object manipulation in a maze by using a swarm of Kilobots. Panel adapted from Reference 59 with permission from IEEE. (*h*) Statistics-based automated control for a swarm of magnetic nanoparticles, including pattern formation control and trajectory tracking control. Panel adapted from Reference 113 with permission from IEEE.

In addition, external disturbances caused by dynamic fluidic forces are also nonlinear, such as the bifurcation effect (36) and pulsatile flow (138). As a result, other advanced closed-loop control methods have been proposed that can be classified into nonlinear control and optimization-based control. With well-modeled system dynamics that account for nonlinearities, many classic nonlinear control approaches have been adopted for controller design, such as adaptive control (61), $\mathcal{H}_\infty$ control (139), and control based on input-to-state stability (140). These nonlinear controllers exhibit better control performance than PID control under uncertainties and disturbances, but their requirements regarding accurate mathematical modeling of the magnetic manipulation system and microrobot restrict their application to only simple microrobots, such as a spherical bead.

Alternatively, optimization-based control also has good robustness to uncertainties and disturbances but does not require precise nonlinearity modeling. For example, minimum variance control can address stochastic uncertainties (141), and model predictive control can reduce tracking error for curved trajectories (128) and suppress motion oscillation (81) owing to its prediction capability. Linear quadratic regulator–based control has also been used for multiple (142) and swarm (113) motion control of magnetic microrobots. For the purpose of generalized disturbance compensation, many disturbance observers can be additionally applied (79, 81).

Unlike motion control of individual and multiple microrobots, pattern control is a special aspect of swarm control. As global inputs are the only feasible method of pattern control, statistics-based approaches have proved effective for Kilobot swarms (59) and nanoparticle swarms (113). This emerging field also embraces new innovations in closed-loop control strategies that do not rely on system modeling, such as fuzzy control (134) and deep learning–based control.

5.2. Feedback Instruments and Signal Processing

The bright-field optical microscope is a traditional instrument to provide feedback information on the environment and state of magnetic microrobots for further motion planning. It has at most submicrometer resolution and is applicable only for on-chip tasks without optical obstructions. Feasible or potential feedback instruments have been explored for closed-loop control for in vitro and in vivo applications. Fluorescence imaging, as a common tool for biomaterial observation, is a good candidate for assisting targeted delivery to cells (81) and in vivo tracking of microrobots (17). Thanks to the easy access to fluorescence microscopes, closed-loop control has been realized (81); however, in vivo closed-loop control remains unsettled. One reason may be difficult integration with the expensive In Vivo Imaging System (IVIS).

Ultrasound is one type of easy-to-access imaging modality for in vivo feedback. Its resolution reaches ~100 μm, and closed-loop control has been demonstrated for microrobots (129). Although the use of ultrasound is theoretically and economically feasible, its low signal-to-noise ratio is far from adequate to detect individual microscale agents in deep tissue. Fortunately, swarm control provides a way forward (143).

Magnetic localization is also effective for in vivo tracking since biological tissue is transparent to magnetic fields. An array of magnetic sensors can be self-constructed for remote sensing of a microrobot inside the body (144, 145), or magnetic sensors can be attached to a microrobot to sense the stronger external field generated by a magnetic manipulation system (146). The major limitation of magnetic localization is that when the device is microscale, the sensor cannot detect its weak field or be attached to it. Clinically, magnetic resonance imaging (MRI) systems have a detection resolution smaller than 100 μm thanks to their strong magnetic field (>1.5 T). In addition to imaging, MRI systems can provide simultaneous motion control for magnetic microrobots. One potential application of an MRI system is to utilize its gradient coils to implement the gradient-pulling method described in Section 3.1 (147).

Other advanced potential in vivo imaging instruments for microrobots have been introduced (3, 148), including computed tomography and positron emission tomography. It is worth mentioning that, more recently, photoacoustic imaging (149) and optical coherence tomography (150) have been applied for navigation guidance of microrobots. Nonetheless, much work remains before these advanced imaging instruments can be used for in vivo closed-loop control of magnetic microrobots.

Many of the above-mentioned feedback instruments directly provide images to a control computer, such as cameras on a microscope, ultrasound, or MRI device. Traditional image-processing methods included in the OpenCV library, such as noise reduction, image segmentation, and feature extraction, can then be used for information extraction. If there are multiple view feedbacks, then the triangulation algorithm can be used for 3D localization. It is well known that lateral observation of microscale objects for 3D tracking is very difficult, for which a new setup based on stereo-holographic diffraction with a self-designed image-processing method provides a solution (151). Optionally, it is also possible to obtain the 3D location of microrobots directly from 2D feedback images. One approach is to calibrate the relationship between feature parameters of the microrobot and its location in the z direction (141); the other is to learn the relationship between nonhuman-defined features and the z location of the microrobot by deep learning (152). Unlike image feedback, several instruments can only give point measurement signals (e.g., magnetic sensors), so that system mathematical modeling is required for 3D localization (144–146). Combining these signal-processing methods with those feedback instruments, researchers have provided many feasible ways to use magnetic microrobots in various environments.

6. SUMMARY AND FUTURE PERSPECTIVES

This article has aimed to introduce readers to motion control in magnetic microrobotics, including the fundamentals, the state of the art, and the current limitations in this field. After approximately 20 years of development, the technologies for motion control of individual magnetic microrobots have become mature. On this basis, several well-understood principles have been proposed for multiagent control. As one can see from **Figure 2**, swarm control of magnetic microrobots is still a young research topic without systematically established theories. Utilizing the underlying motion principles of magnetic microrobotics, the robotics and control communities can pave the way to applications by designing and implementing various feedback instruments and closed-loop control systems. However, magnetic microrobotic systems have not yet fulfilled their promise for in vivo automatic navigation for applications in complex environments. Several areas of potential future research can help meet this ultimate goal:

- Multifunctional magnetic microrobots: Innovative designs with new functions (e.g., force sensing and biosensing) would be a promising future direction that can expand the applications of magnetic microrobots.
- Fundamentals of swarm control in magnetic microrobotics: Meaningful challenges that need to be tackled include establishing systematic design methodologies for swarm control, developing methods for swarm navigation in 3D space, and bringing intelligence to magnetic microswarms with good adaptability to complex environments and high autonomy levels.
- Motion control in biological media: Many common fluids in the human body are non-Newtonian, including sputum, saliva, and vitreous humor, and biological media usually contain inhomogeneous macromolecules, cells, and so on. These two facts increase the difficulty of microrobot motion, which is the key problem to be solved for microrobotic delivery tasks in these media.

- Advanced intelligent control strategies for magnetic microrobotic navigation in complex and dynamic environments: Current microrobot control tasks often assume a simple and static environment, which is very different from real-world environments. This objective requires identifying complex environments and microrobot states, performing dynamic motion planning and control, and so on. Deep learning–based methods have boosted applications in many fields and provide substantial opportunities for innovation in magnetic microrobot motion control.
- System integration with real-time in vivo feedback and/or auxiliary medical tools: Although various feedback instruments have been introduced for in vivo microrobotic feedback, only a few have been integrated with a magnetic manipulation system to make the microrobots work in a closed-loop or autonomous manner. On the other hand, to facilitate microrobotic delivery to deep and narrow spaces, medical minimally invasive tools can be integrated for the deployment of micro- and nanorobots, such as endoscope- and catheter-assisted microrobotic delivery.

DISCLOSURE STATEMENT

The authors are not aware of any affiliations, memberships, funding, or financial holdings that might be perceived as affecting the objectivity of this review.

ACKNOWLEDGMENTS

The authors acknowledge funding support from the Hong Kong Research Grants Council (RGC) through the Joint Laboratory Funding Scheme (JLFS/E-402/18) and General Research Fund (14218516), the Hong Kong Innovation and Technology Commission through the Innovation and Technology Fund (MRP/036/18X and ITS/374/18FP), the Chinese University of Hong Kong Impact Postdoctoral Fellowship Scheme, and the Research Sustainability of Major RGC Funding Scheme (3133228). L.Z. would also like to thank the Multi-Scale Medical Robotics Center, InnoHK, Hong Kong Science Park, for its support.

LITERATURE CITED

1. Abbott JJ, Nagy Z, Beyeler F, Nelson BJ. 2007. Robotics in the small, part I: microbotics. *IEEE Robot. Autom. Mag.* 14(2):92–103
2. Diller E, Sitti M. 2013. Micro-scale mobile robotics. *Found. Trends Robot.* 2:143–259
3. Nelson BJ, Kaliakatsos IK, Abbott JJ. 2010. Microrobots for minimally invasive medicine. *Annu. Rev. Biomed. Eng.* 12:55–85
4. Sitti M, Ceylan H, Hu W, Giltinan J, Turan M, et al. 2015. Biomedical applications of untethered mobile milli/microrobots. *Proc. IEEE* 103:205–24
5. Xu T, Gao W, Xu LP, Zhang X, Wang S. 2017. Fuel-free synthetic micro-/nanomachines. *Adv. Mater.* 29:1603250
6. Palima D, Glückstad J. 2013. Gearing up for optical microrobotics: micromanipulation and actuation of synthetic microstructures by optical forces. *Laser Photonics Rev.* 7:478–94
7. Karshalev E, Esteban-Fernandez de Avila B, Wang J. 2018. Micromotors for "chemistry-on-the-fly." *J. Am. Chem. Soc.* 140:3810–20
8. Rao KJ, Li F, Meng L, Zheng H, Cai F, Wang W. 2015. A force to be reckoned with: a review of synthetic microswimmers powered by ultrasound. *Small* 11:2836–46
9. Donald BR, Levey CG, McGray CD, Paprotny I, Rus D. 2006. An untethered, electrostatic, globally controllable MEMS micro-robot. *J. Microelectromech. Syst.* 15:1–15
10. Peyer KE, Zhang L, Nelson BJ. 2013. Bio-inspired magnetic swimming microrobots for biomedical applications. *Nanoscale* 5:1259–72

11. Felfoul O, Mohammadi M, Taherkhani S, De Lanauze D, Xu YZ, et al. 2016. Magneto-aerotactic bacteria deliver drug-containing nanoliposomes to tumour hypoxic regions. *Nat. Nanotechnol.* 11:941–47
12. Li J, Li X, Luo T, Wang R, Liu C, et al. 2018. Development of a magnetic microrobot for carrying and delivering targeted cells. *Sci. Robot.* 3:eaat8829
13. Zhang Y, Zhang L, Yang L, Vong CI, Chan KF, et al. 2019. Real-time tracking of fluorescent magnetic spore–based microrobots for remote detection of *C. diff* toxins. *Sci. Adv.* 5:eaau9650
14. Wang X, Ho C, Tsatskis Y, Law J, Zhang Z, et al. 2019. Intracellular manipulation and measurement with multipole magnetic tweezers. *Sci. Robot.* 4:eaav6180
15. Wu Z, Troll J, Jeong HH, Wei Q, Stang M, et al. 2018. A swarm of slippery micropropellers penetrates the vitreous body of the eye. *Sci. Adv.* 4:eaat4388
16. Yu J, Jin D, Chan KF, Wang Q, Yuan K, Zhang L. 2019. Active generation and magnetic actuation of microrobotic swarms in bio-fluids. *Nat. Commun.* 10:5631
17. Servant A, Qiu F, Mazza M, Kostarelos K, Nelson BJ. 2015. Controlled in vivo swimming of a swarm of bacteria-like microrobotic flagella. *Adv. Mater.* 27:2981–88
18. Abbott JJ, Diller E, Petruska AJ. 2019. Magnetic methods in robotics. *Annu. Rev. Control Robot. Auton. Syst.* 3:57–90
19. Xu T, Yu J, Yan X, Choi H, Zhang L. 2015. Magnetic actuation based motion control for microrobots: an overview. *Micromachines* 6:1346–64
20. Yang L, Du X, Yu E, Jin D, Zhang L. 2019. DeltaMag: an electromagnetic manipulation system with parallel mobile coils. In *2019 IEEE International Conference on Robotics and Automation*, pp. 9814–20. Piscataway, NJ: IEEE
21. Hu C, Pané S, Nelson BJ. 2018. Soft micro- and nanorobotics. *Annu. Rev. Control Robot. Auton. Syst.* 1:53–75
22. Alapan Y, Yasa O, Yigit B, Yasa IC, Erkoc P, Sitti M. 2019. Microrobotics and microorganisms: biohybrid autonomous cellular robots. *Annu. Rev. Control Robot. Auton. Syst.* 2:205–30
23. Zhang Z, Wang X, Liu J, Dai C, Sun Y. 2019. Robotic micromanipulation: fundamentals and applications. *Annu. Rev. Control Robot. Auton. Syst.* 2:181–203
24. Wautelet M. 2001. Scaling laws in the macro-, micro- and nanoworlds. *Eur. J. Phys.* 22:601–11
25. Abbott JJ, Peyer KE, Lagomarsino MC, Zhang L, Dong L, et al. 2009. How should microrobots swim? *Int. J. Robot. Res.* 28:1434–47
26. Petruska AJ, Nelson BJ. 2015. Minimum bounds on the number of electromagnets required for remote magnetic manipulation. *IEEE Trans. Robot.* 31:714–22
27. Mahoney AW, Abbott JJ. 2016. Five-degree-of-freedom manipulation of an untethered magnetic device in fluid using a single permanent magnet with application in stomach capsule endoscopy. *Int. J. Robot. Res.* 35:129–47
28. Petruska AJ, Abbott JJ. 2012. Optimal permanent-magnet geometries for dipole field approximation. *IEEE Trans. Magn.* 49:811–19
29. Salehizadeh M, Diller E. 2017. Two-agent formation control of magnetic microrobots in two dimensions. *J. Micro-Bio Robot.* 12:9–19
30. Wang Q, Yang L, Wang B, Yu E, Yu J, Zhang L. 2018. Collective behavior of reconfigurable magnetic droplets via dynamic self-assembly. *ACS Appl. Mater. Interfaces* 11:1630–37
31. White FM. 2015. *Fluid Mechanics*. New York: McGraw-Hill
32. Loth E. 2008. Drag of non-spherical solid particles of regular and irregular shape. *Powder Technol.* 182:342–53
33. Finn R. 1953. Determination of the drag on a cylinder at low Reynolds numbers. *J. Appl. Phys.* 24:771–73
34. Yu J, Xu T, Lu Z, Vong CI, Zhang L. 2017. On-demand disassembly of paramagnetic nanoparticle chains for microrobotic cargo delivery. *IEEE Trans. Robot.* 33:1213–25
35. Lee H, Balachandar S. 2010. Drag and lift forces on a spherical particle moving on a wall in a shear flow at finite *Re*. *J. Fluid Mech.* 657:89–125
36. Arcese L, Fruchard M, Ferreira A. 2011. Endovascular magnetically guided robots: navigation modeling and optimization. *IEEE Trans. Biomed. Eng.* 59:977–87
37. Liu Q, Prosperetti A. 2010. Wall effects on a rotating sphere. *J. Fluid Mech.* 657:1–21

38. Kehlenbeck R, Felice RD. 1999. Empirical relationships for the terminal settling velocity of spheres in cylindrical columns. *Chem. Eng. Technol.* 22:303–8
39. Stalnaker JF, Hussey R. 1979. Wall effects on cylinder drag at low Reynolds number. *Phys. Fluids* 22:603–13
40. Samantaray SK, Mohapatra SS, Munshi B. 2017. A numerical study of the wall effects for Newtonian fluid flow over a cone. *Eng. Sci. Technol. Int. J.* 20:1662–75
41. Tierno P, Golestanian R, Pagonabarraga I, Sagués F. 2008. Controlled swimming in confined fluids of magnetically actuated colloidal rotors. *Phys. Rev. Lett.* 101:218304
42. Yu J, Yang L, Zhang L. 2018. Pattern generation and motion control of a vortex-like paramagnetic nanoparticle swarm. *Int. J. Robot. Res.* 37:912–30
43. Yang L, Zhang Y, Wang Q, Zhang L. 2019. An automated microrobotic platform for rapid detection of *C. diff* toxins. *IEEE Trans. Biomed. Eng.* 67:1517–27
44. Pieters R, Tung HW, Charreyron S, Sargent DF, Nelson BJ. 2015. RodBot: a rolling microrobot for micromanipulation. In *2015 IEEE Conference on Robotics and Automation*, pp. 4042–47. Piscataway, NJ: IEEE
45. Zhou Q, Petit T, Choi H, Nelson BJ, Zhang L. 2017. Dumbbell fluidic tweezers for dynamical trapping and selective transport of microobjects. *Adv. Funct. Mater.* 27:1604571
46. Paris A, Decanini D, Hwang G. 2018. On-chip multimodal vortex trap micro-manipulator with multi-stage bi-helical micro-swimmer. *Sens. Actuat. A* 276:118–24
47. Kaiser A, Snezhko A, Aranson IS. 2017. Flocking ferromagnetic colloids. *Sci. Adv.* 3:e1601469
48. Xie H, Sun M, Fan X, Lin Z, Chen W, et al. 2019. Reconfigurable magnetic microrobot swarm: multimode transformation, locomotion, and manipulation. *Sci. Robot.* 4:eaav8006
49. Grzybowski BA, Jiang X, Stone HA, Whitesides GM. 2001. Dynamic, self-assembled aggregates of magnetized, millimeter-sized objects rotating at the liquid-air interface: macroscopic, two-dimensional classical artificial atoms and molecules. *Phys. Rev. E* 64:011603
50. Chwang AT, Wu TYT. 1974. Hydromechanics of low-Reynolds-number flow. Part 1. Rotation of axisymmetric prolate bodies. *J. Fluid Mech.* 63:607–22
51. Qiu T, Lee TC, Mark AG, Morozov KI, Münster R, et al. 2014. Swimming by reciprocal motion at low Reynolds number. *Nat. Commun.* 5:5119
52. Pawashe C, Floyd S, Sitti M. 2009. Modeling and experimental characterization of an untethered magnetic micro-robot. *Int. J. Robot. Res.* 28:1077–94
53. Diller E, Floyd S, Pawashe C, Sitti M. 2011. Control of multiple heterogeneous magnetic microrobots in two dimensions on nonspecialized surfaces. *IEEE Trans. Robot.* 28:172–82
54. Steager EB, Selman Sakar M, Magee C, Kennedy M, Cowley A, Kumar V. 2013. Automated biomanipulation of single cells using magnetic microrobots. *Int. J. Robot. Res.* 32:346–59
55. Frutiger DR, Vollmers K, Kratochvil BE, Nelson BJ. 2010. Small, fast, and under control: wireless resonant magnetic micro-agents. *Int. J. Robot. Res.* 29:613–36
56. Diller E, Pawashe C, Floyd S, Sitti M. 2011. Assembly and disassembly of magnetic mobile micro-robots towards deterministic 2-D reconfigurable micro-systems. *Int. J. Robot. Res.* 30:1667–80
57. Kantaros Y, Johnson BV, Chowdhury S, Cappelleri DJ, Zavlanos MM. 2018. Control of magnetic microrobot teams for temporal micromanipulation tasks. *IEEE Trans. Robot.* 34:1472–89
58. Shahrokhi S, Shi J, Isichei B, Becker AT. 2019. Exploiting nonslip wall contacts to position two particles using the same control input. *IEEE Trans. Robot.* 35:577–88
59. Shahrokhi S, Lin L, Ertel C, Wan M, Becker AT. 2017. Steering a swarm of particles using global inputs and swarm statistics. *IEEE Trans. Robot.* 34:207–19
60. Dogangil G, Ergeneman O, Abbott JJ, Pané S, Hall H, et al. 2008. Toward targeted retinal drug delivery with wireless magnetic microrobots. In *2008 IEEE/RSJ International Conference on Intelligent Robots and Systems*, pp. 1921–26. Piscataway, NJ: IEEE
61. Arcese L, Fruchard M, Ferreira A. 2013. Adaptive controller and observer for a magnetic microrobot. *IEEE Trans. Robot.* 29:1060–67
62. Zhang L, Abbott JJ, Dong L, Kratochvil BE, Bell D, Nelson BJ. 2009. Artificial bacterial flagella: fabrication and magnetic control. *Appl. Phys. Lett.* 94:064107

63. Qiu F, Zhang L, Peyer KE, Casarosa M, Franco-Obregón A, et al. 2014. Noncytotoxic artificial bacterial flagella fabricated from biocompatible ORMOCOMP and iron coating. *J. Mater. Chem. B* 2:357–62
64. Tottori S, Zhang L, Qiu F, Krawczyk KK, Franco-Obregón A, Nelson BJ. 2012. Magnetic helical micromachines: fabrication, controlled swimming, and cargo transport. *Adv. Mater.* 24:811–16
65. Huang HW, Uslu FE, Katsamba P, Lauga E, Selman Sakar M, Nelson B. 2019. Adaptive locomotion of artificial microswimmers. *Sci. Adv.* 5:eaau1532
66. Khalil IS, Hafez M, Klingnert A, Scheggi S, Adel B, Misra S. 2018. Near surface effects on the flagellar propulsion of soft robotic sperms. In *2018 7th IEEE International Conference on Biomedical Robotics and Biomechatronics*, pp. 384–89. Piscataway, NJ: IEEE
67. Jang B, Gutman E, Stucki N, Seitz BF, Wendel-García PD, et al. 2015. Undulatory locomotion of magnetic multilink nanoswimmers. *Nano Lett.* 15:4829–33
68. Tung HW, Maffioli M, Frutiger DR, Sivaraman KM, Pané S, Nelson BJ. 2013. Polymer-based wireless resonant magnetic microrobots. *IEEE Trans. Robot.* 30:26–32
69. Hu W, Lum GZ, Mastrangeli M, Sitti M. 2018. Small-scale soft-bodied robot with multimodal locomotion. *Nature* 554:81–85
70. Mathieu JB, Beaudoin G, Martel S. 2006. Method of propulsion of a ferromagnetic core in the cardiovascular system through magnetic gradients generated by an MRI system. *IEEE Trans. Biomed. Eng.* 53:292–99
71. Choi H, Choi J, Jeong S, Yu C, Park Jo, Park S. 2009. Two-dimensional locomotion of a microrobot with a novel stationary electromagnetic actuation system. *Smart Mater. Struct.* 18:115017
72. Kummer MP, Abbott JJ, Kratochvil BE, Borer R, Sengul A, Nelson BJ. 2010. OctoMag: an electromagnetic system for 5-DOF wireless micromanipulation. *IEEE Trans. Robot.* 26:1006–17
73. Yan X, Zhou Q, Vincent M, Deng Y, Yu J, et al. 2017. Multifunctional biohybrid magnetite microrobots for imaging-guided therapy. *Sci. Robot.* 2:eaaq1155
74. Xu T, Hwang G, Andreff N, Régnier S. 2015. Planar path following of 3-D steering scaled-up helical microswimmers. *IEEE Trans. Robot.* 31:117–27
75. Medina-Sánchez M, Schwarz L, Meyer AK, Hebenstreit F, Schmidt OG. 2015. Cellular cargo delivery: toward assisted fertilization by sperm-carrying micromotors. *Nano Lett.* 16:555–61
76. Magdanz V, Sanchez S, Schmidt OG. 2013. Development of a sperm-flagella driven micro-bio-robot. *Adv. Mater.* 25:6581–88
77. Khalil IS, Magdanz V, Hamed Y, Toubar M, Misra S, Klingner A. 2019. Characterization of flagellar propulsion of soft microrobotic sperm in a viscous heterogeneous medium. *Front. Robot. AI* 6:65
78. Pieters RS, Tung HW, Sargent DF, Nelson BJ. 2014. Non-contact manipulation for automated protein crystal harvesting using a rolling microrobot. *IFAC Proc. Vol.* 47:7480–85
79. Yang L, Wang Q, Zhang L. 2018. Model-free trajectory tracking control of two-particle magnetic microrobot. *IEEE Trans. Nanotechnol.* 17:697–700
80. Fan X, Sun M, Lin Z, Song J, He Q, et al. 2018. Automated noncontact micromanipulation using magnetic swimming microrobots. *IEEE Trans. Nanotechnol.* 17:666–69
81. Yang L, Zhang Y, Wang Q, Chan K, Zhang L. 2020. Automated control of magnetic spore-based microrobot using fluorescence imaging for targeted delivery with cellular resolution. *IEEE Trans. Autom. Sci. Eng.* 17:490–501
82. Floyd S, Diller E, Pawashe C, Sitti M. 2011. Control methodologies for a heterogeneous group of untethered magnetic micro-robots. *Int. J. Robot. Res.* 30:1553–65
83. Diller E, Giltinan J, Sitti M. 2013. Independent control of multiple magnetic microrobots in three dimensions. *Int. J. Robot. Res.* 32:614–31
84. Wong D, Steager EB, Kumar V. 2016. Independent control of identical magnetic robots in a plane. *IEEE Robot. Autom. Lett.* 1:554–61
85. Denasi A, Misra S. 2017. Independent and leader–follower control for two magnetic micro-agents. *IEEE Robot. Autom. Lett.* 3:218–25
86. Ongaro F, Pane S, Scheggi S, Misra S. 2019. Design of an electromagnetic setup for independent three-dimensional control of pairs of identical and nonidentical microrobots. *IEEE Trans. Robot.* 35:174–83

87. Becker A, Ou Y, Kim P, Kim MJ, Julius A. 2013. Feedback control of many magnetized *Tetrahymena pyriformis* cells by exploiting phase inhomogeneity. In *2013 IEEE/RSJ International Conference on Intelligent Robots and Systems*, pp. 3317–23. Piscataway, NJ: IEEE
88. Salchizadeh M, Li Z, Diller E. 2019. Independent position control of two magnetic microrobots via rotating magnetic field in two dimensions. In *2019 International Conference on Manipulation, Automation and Robotics at Small Scales*. Piscataway, NJ: IEEE. **https://doi.org/10.1109/MARSS.2019.8860954**
89. Wang X, Hu C, Schurz L, De Marco C, Chen X, et al. 2018. Surface-chemistry-mediated control of individual magnetic helical microswimmers in a swarm. *ACS Nano* 12:6210–17
90. Mahoney AW, Nelson ND, Peyer KE, Nelson BJ, Abbott JJ. 2014. Behavior of rotating magnetic microrobots above the step-out frequency with application to control of multi-microrobot systems. *Appl. Phys. Lett.* 104:144101
91. Tottori S, Sugita N, Kometani R, Ishihara S, Mitsuishi M. 2011. Selective control method for multiple magnetic helical microrobots. *J. Micro-Nano Mech.* 6:89–95
92. Kawaguchi T, Inoue Y, Ikeuchi M, Ikuta K. 2018. Independent actuation and master-slave control of multiple micro magnetic actuators. In *2018 IEEE Micro Electro Mechanical Systems*, pp. 190–93. Piscataway, NJ: IEEE
93. Nelson ND, Abbott JJ. 2015. Generating two independent rotating magnetic fields with a single magnetic dipole for the propulsion of untethered magnetic devices. In *2015 IEEE Conference on Robotics and Automation*, pp. 4056–61. Piscataway, NJ: IEEE
94. Rahmer J, Stehning C, Gleich B. 2017. Spatially selective remote magnetic actuation of identical helical micromachines. *Sci. Robot.* 2:eaal2845
95. Tottori S, Zhang L, Peyer KE, Nelson BJ. 2013. Assembly, disassembly, and anomalous propulsion of microscopic helices. *Nano Lett.* 13:4263–68
96. Khalil IS, Tabak AF, Hamed Y, Tawakol M, Klingner A, et al. 2018. Independent actuation of two-tailed microrobots. *IEEE Robot. Autom. Lett.* 3:1703–10
97. Kratochvil BE, Frutiger D, Vollmers K, Nelson BJ. 2009. Visual servoing and characterization of resonant magnetic actuators for decoupled locomotion of multiple untethered mobile microrobots. In *2009 IEEE International Conference on Robotics and Automation*, pp. 1010–15. Piscataway, NJ: IEEE
98. Martel S, Mohammadi M. 2010. Using a swarm of self-propelled natural microrobots in the form of flagellated bacteria to perform complex micro-assembly tasks. In *2010 IEEE International Conference on Robotics and Automation*, pp. 500–5. Piscataway, NJ: IEEE
99. Loghin D, Tremblay C, Mohammadi M, Martel S. 2017. Exploiting the responses of magnetotactic bacteria robotic agents to enhance displacement control and swarm formation for drug delivery platforms. *Int. J. Robot. Res.* 36:1195–210
100. Vach PJ, Walker D, Fischer P, Fratzl P, Faivre D. 2017. Pattern formation and collective effects in populations of magnetic microswimmers. *J. Phys. D* 50:11LT03
101. Tasci T, Herson P, Neeves K, Marr D. 2016. Surface-enabled propulsion and control of colloidal microwheels. *Nat. Commun.* 7:10225
102. Martinez-Pedrero F, Cebers A, Tierno P. 2016. Dipolar rings of microscopic ellipsoids: magnetic manipulation and cell entrapment. *Phys. Rev. Appl.* 6:034002
103. Gao Y, van Reenen A, Hulsen MA, de Jong AM, Prins MW, den Toonder JM. 2013. Disaggregation of microparticle clusters by induced magnetic dipole–dipole repulsion near a surface. *Lab Chip* 13:1394–401
104. Diller E, Giltinan J, Lum GZ, Ye Z, Sitti M. 2016. Six-degree-of-freedom magnetic actuation for wireless microrobotics. *Int. J. Robot. Res.* 35:114–28
105. Koyasu S, Shirakihara Y. 1984. *Caulobacter crescentus* flagellar filament has a right-handed helical form. *J. Mol. Biol.* 173:125–30
106. Purcell EM. 1977. Life at low Reynolds number. *Am. J. Phys.* 45:3–11
107. Li T, Li J, Zhang H, Chang X, Song W, et al. 2016. Magnetically propelled fish-like nanoswimmers. *Small* 12:6098–105
108. Rubenstein M, Cornejo A, Nagpal R. 2014. Programmable self-assembly in a thousand-robot swarm. *Science* 345:795–99

109. Becker A, Habibi G, Werfel J, Rubenstein M, McLurkin J. 2013. Massive uniform manipulation: controlling large populations of simple robots with a common input signal. In *2013 IEEE/RSJ International Conference on Intelligent Robots and Systems*, pp. 520–27. Piscataway, NJ: IEEE
110. Belkin M, Snezhko A, Aranson I, Kwok WK. 2007. Driven magnetic particles on a fluid surface: pattern assisted surface flows. *Phys. Rev. Lett.* 99:158301
111. Snezhko A, Aranson IS. 2011. Magnetic manipulation of self-assembled colloidal asters. *Nat. Mater.* 10:698–703
112. Yu J, Wang B, Du X, Wang Q, Zhang L. 2018. Ultra-extensible ribbon-like magnetic microswarm. *Nat. Commun.* 9:3260
113. Yang L, Yu J, Zhang L. 2020. Statistics-based automated control for a swarm of paramagnetic nanoparticles in 2-D space. *IEEE Trans. Robot.* 36:254–70
114. Becker AT. 2017. Controlling swarms of robots with global inputs: breaking symmetry. In *Microbiorobotics: Biologically Inspired Microscale Robotic Systems*, ed. M Kim, AA Julius, U Key, pp. 3–20. Amsterdam: Elsevier. 2nd ed.
115. Mandal P, Chopra V, Ghosh A. 2015. Independent positioning of magnetic nanomotors. *ACS Nano* 9:4717–25
116. Ceylan H, Giltinan J, Kozielski K, Sitti M. 2017. Mobile microrobots for bioengineering applications. *Lab Chip* 17:1705–24
117. Yan J, Bloom M, Bae SC, Luijten E, Granick S. 2012. Linking synchronization to self-assembly using magnetic Janus colloids. *Nature* 491:578–81
118. Mohoric T, Kokot G, Osterman N, Snezhko A, Vilfan A, et al. 2016. Dynamic assembly of magnetic colloidal vortices. *Langmuir* 32:5094–101
119. Martinez-Pedrero F, Tierno P. 2015. Magnetic propulsion of self-assembled colloidal carpets: efficient cargo transport via a conveyor-belt effect. *Phys. Rev. Appl.* 3:051003
120. Wang W, Giltinan J, Zakharchenko S, Sitti M. 2017. Dynamic and programmable self-assembly of micro-rafts at the air-water interface. *Sci. Adv.* 3:e1602522
121. Wang B, Chan KF, Yu J, Wang Q, Yang L, et al. 2018. Reconfigurable swarms of ferromagnetic colloids for enhanced local hyperthermia. *Adv. Funct. Mater.* 28:1705701
122. Wang Q, Yu J, Yuan K, Yang L, Jin D, Zhang L. 2019. Disassembly and spreading of magnetic nanoparticle clusters on uneven surfaces. *Appl. Mater. Today* 18:100489
123. Dong X, Sitti M. 2020. Controlling two-dimensional collective formation and cooperative behavior of magnetic microrobot swarms. *Int. J. Robot. Res.* 39:617–38
124. Yigit B, Alapan Y, Sitti M. 2019. Programmable collective behavior in dynamically self-assembled mobile microrobotic swarms. *Adv. Sci.* 6:1801837
125. Chao Q, Yu J, Dai C, Xu T, Zhang L, et al. 2016. Steering micro-robotic swarm by dynamic actuating fields. In *2016 IEEE International Conference on Robotics and Automation*, pp. 5230–35. Piscataway, NJ: IEEE
126. Shahrokhi S, Becker AT. 2015. Stochastic swarm control with global inputs. In *2015 IEEE/RSJ International Conference on Intelligent Robots and Systems*, pp. 421–27. Piscataway, NJ: IEEE
127. Martel S, Taherkhani S, Tabrizian M, Mohammadi M, de Lanauze D, Felfoul O. 2014. Computer 3D controlled bacterial transports and aggregations of microbial adhered nano-components. *J. Micro-Bio Robot.* 9:23–28
128. Pieters R, Lombriser S, Alvarez-Aguirre A, Nelson BJ. 2016. Model predictive control of a magnetically guided rolling microrobot. *IEEE Robot. Autom. Lett.* 1:455–60
129. Khalil IS, Ferreira P, Eleutério R, de Korte CL, Misra S. 2014. Magnetic-based closed-loop control of paramagnetic microparticles using ultrasound feedback. In *2014 IEEE International Conference on Robotics and Automation*, pp. 3807–12. Piscataway, NJ: IEEE
130. Huang L, Rogowski L, Kim MJ, Becker AT. 2017. Path planning and aggregation for a microrobot swarm in vascular networks using a global input. In *2017 IEEE/RSJ International Conference on Intelligent Robots and Systems*, pp. 414–20. Piscataway, NJ: IEEE
131. Xie H, Fan X, Sun M, Lin Z, He Q, Sun L. 2019. Programmable generation and motion control of a snakelike magnetic microrobot swarm. *IEEE/ASME Trans. Mechatron.* 24:902–12

132. Kim H, Cheang UK, Kim MJ. 2017. Autonomous dynamic obstacle avoidance for bacteria-powered microrobots (BPMs) with modified vector field histogram. *PLOS ONE* 12:e0185744
133. Li X, Chen S, Liu C, Cheng SH, Wang Y, Sun D. 2018. Development of a collision-avoidance vector based control algorithm for automated in-vivo transportation of biological cells. *Automatica* 90:147–56
134. Yang L, Yu J, Zhang L. 2020. A mobile paramagnetic nanoparticle swarm with automatic shape deformation control. In *2020 IEEE International Conference on Robotics and Automation*, pp. 9230–36. Piscataway, NJ: IEEE
135. Tamaz S, Gourdeau R, Chanu A, Mathieu JB, Martel S. 2008. Real-time MRI-based control of a ferromagnetic core for endovascular navigation. *IEEE Trans. Biomed. Eng.* 55:1854–63
136. Lucarini G, Palagi S, Levi A, Mazzolai B, Dario P, et al. 2014. Navigation of magnetic microrobots with different user interaction levels. *IEEE Trans. Autom. Sci. Eng.* 11:818–27
137. Bergeles C, Kratochvil BE, Nelson BJ. 2012. Visually servoing magnetic intraocular microdevices. *IEEE Trans. Robot.* 28:798–809
138. Sadelli L, Fruchard M, Ferreira A. 2016. 2D observer-based control of a vascular microrobot. *IEEE Trans. Autom. Control* 62:2194–206
139. Marino H, Bergeles C, Nelson BJ. 2013. Robust electromagnetic control of microrobots under force and localization uncertainties. *IEEE Trans. Autom. Sci. Eng.* 11:310–16
140. Ma W, Li J, Niu F, Ji H, Sun D. 2017. Robust control to manipulate a microparticle with electromagnetic coil system. *IEEE Trans. Ind. Electron.* 64:8566–77
141. Zhang Z, Long F, Menq CH. 2012. Three-dimensional visual servo control of a magnetically propelled microscopic bead. *IEEE Trans. Robot.* 29:373–82
142. Mellal L, Folio D, Belharet K, Ferreira A. 2016. Optimal control of multiple magnetic microbeads navigating in microfluidic channels. In *2016 IEEE International Conference on Robotics and Automation*, pp. 1921–26. Piscataway, NJ: IEEE
143. Wang Q, Yang L, Yu J, Vong CI, Chiu PWY, Zhang L. 2018. Magnetic navigation of a rotating colloidal swarm using ultrasound images. In *2018 IEEE/RSJ International Conference on Intelligent Robots and Systems*, pp. 5380–85. Piscataway, NJ: IEEE
144. Hu C, Meng MQH, Mandal M. 2005. Efficient magnetic localization and orientation technique for capsule endoscopy. *Int. J. Inf. Acquis.* 2:23–36
145. Son D, Dong X, Sitti M. 2018. A simultaneous calibration method for magnetic robot localization and actuation systems. *IEEE Trans. Robot.* 35:343–52
146. Popek KM, Hermans T, Abbott JJ. 2017. First demonstration of simultaneous localization and propulsion of a magnetic capsule in a lumen using a single rotating magnet. In *2017 IEEE International Conference on Robotics and Automation*, pp. 1154–60. Piscataway, NJ: IEEE
147. Martel S, Mathieu JB, Felfoul O, Chanu A, Aboussouan E, et al. 2007. Automatic navigation of an untethered device in the artery of a living animal using a conventional clinical magnetic resonance imaging system. *Appl. Phys. Lett.* 90:114105
148. Martel S. 2013. Microrobotics in the vascular network: present status and next challenges. *J. Micro-Bio Robot.* 8:41–52
149. Wu Z, Li L, Yang Y, Hu P, Li Y, et al. 2019. A microrobotic system guided by photoacoustic computed tomography for targeted navigation in intestines in vivo. *Sci. Robot.* 4:eaax0613
150. Li D, Dong D, Lam W, Xing L, Wei T, Sun D. 2019. Automated in vivo navigation of magnetic-driven microrobots using OCT imaging feedback. *IEEE Trans. Biomed. Eng.* 67:2349–58
151. Mohanty S, Hong A, Alcantara C, Petruska AJ, Nelson BJ. 2017. Stereo holographic diffraction based tracking of microrobots. *IEEE Robot. Autom. Lett.* 3:567–72
152. Grammatikopoulou M, Yang GZ. 2019. Three-dimensional pose estimation of optically transparent microrobots. *IEEE Robot. Autom. Lett.* 5:72–79

Annual Review of Control, Robotics, and Autonomous Systems

Volume 4, 2021

Contents

Errata

An online log of corrections to *Annual Review of Control, Robotics, and Autonomous Systems* articles may be found at http://www.annualreviews.org/errata/control